RESEARCH ARTICLE

Insights into the $Hf_nNb_2O_{2n+5}$ homologous phases from experimental, first-principle, and force-field studies

Andreas Herklotz[1] | **Kyle Martin Grove[2]** | **Michael S. Bowen[2]** |
Ryan Mc Quade[2] | **Kristin Elizabeth Tippey[3]** | **David P. Cann[2]**

[1]Institute for Physics,
Martin-Luther-University
Halle-Wittenberg, Halle, Germany

[2]School of Mechanical, Industrial, and
Manufacturing Engineering, Oregon State
University, Corvallis, Oregon, USA

[3]Helmholtz-Zentrum
Dresden-Rossendorf, Dresden, Germany

Correspondence
Andreas Herklotz, Institute for Physics,
Martin-Luther-University
Halle-Wittenberg, Halle, Germany.
Email: herklotza@gmail.com

Funding information
Deutsche Forschungsgemeinschaft,
Grant/Award Number: HE8737/1-1;
Scientific User Facilities Division, Office
of Basic Energy Sciences, U.S. Department
of Energy

Abstract

Different outcomes have been presented on the preparation of high-temperature ceramic $A_nB_2O_{2n+5}$ (A = Hf, Zr and B = Nb, Ta). Considering the importance of these materials as refractories, the stability range of the A = Hf and B = Nb compound is experimentally determined by preparing ceramics via solid-state synthesis and analyzing their phase compositions. Then, the density functional theory was used to study the stability of the homologous series versus decomposition to the parent compounds of HfO_2 and Nb_2O_5. A good agreement with the experimental values is found. In order to improve the theoretical data further, an interatomic potential based on the first-principle calculations is developed and applied to larger supercell structures. These force-field calculations confirm the stability of the homologous series versus a solid solution. The calculations also allow us to study cation order and periodic compositional modulation.

KEYWORDS
molecular dynamics, solid solutions, structure, ultra-high temperature ceramics

1 | INTRODUCTION

Refractory materials find extensive use in a wide spectrum of high-temperature applications. In the past decade, research on refractories has increasingly shifted to advanced materials systems which must withstand high temperatures and aggressive environments. These systems possess multifunctional properties that meet requirements in thermal barrier coatings or semiconductor devices.[1–3] In addition, the AO_2–B_2O_5 system class with A = (Zr, Hf) and B = (Nb, Ta) has seen revived interest after the discovery of ferroelectricity in orthorhombic HfO_2 and increased interest in entropy-stabilized oxides.[4–6] A hallmark feature of this material class is the formation of

an orthorhombic $A_6B_2O_{17}$ phase with increased oxidation resistance, ultra-high melting temperatures, and low thermal conductivity.[7]

The crystal structure of $A_6B_2O_{17}$ was first described in the 1970s, but the subsequent work has shown that a complete and satisfactory structural characterization is difficult. In a simplified picture, $A_6B_2O_{17}$ can be seen as part of a homologous series with $A_nB_2O_{2n+5}$ which can be described as α-PbO_2-homeotypic superstructures of this unit cell.[8] It was found that members of this homologous series appear to be stable for $5 \leq n \leq 8$ for all cation combinations, and a solid solution within these limits would form by varying the content of the series members. However, it was soon realized by Galy and Roth that

the compounds within the $A_6B_2O_{17}$ phase space possess superstructure X-ray diffraction peaks, whose positions vary smoothly with composition, which is incoherent with the former model.[9] A refined description of the structural characteristics of $A_6B_2O_{17}$ acknowledges that the cation and oxygen ions basically form independent sublattices that allow for incommensurate compositional modulation. In this revised picture, the whole $A_6B_2O_{17}$ phase space can be seen as a coherent material system, where compositional changes are accommodated by changes in the modulation vectors of the cation and anion sublattices.[10,11]

Although this new crystal structure model solves many of the shortcomings of the simple homologous series picture, further work is needed to fully understand all nuances in the observed experimental data. For example, the comparison of the work of McCormack et al.[7] and Thompson et al.[10] suggests that the stability region of $Hf_nTa_2O_{2n+5}$ is significantly wider than for $Zr_nNb_2O_{2n+5}$. Moreover, due to the similar X-ray scattering factors of Zr and Nb, as well as Hf and Ta, the presence of cation disorder in these two compounds could not be ruled out. A model framework that helps to satisfyingly reproduce the common futures of $A_nB_2O_{2n+5}$, but also provides insights into the differences between the different systems, would be beneficial.

In this paper, we first determine stability limits of the $Hf_6Nb_2O_{17}$ system and investigated its special diffraction features. We then apply various theoretical methods to calculate the stability limits from first-principles, namely density functional theory (DFT) and force-field calculations. We find a good agreement between experimental and theoretical data, which suggests that this theoretical framework can be used to predict other features of the other $A_nB_2O_{2n+5}$ systems, where A = Hf, Nb and B = Nb, Ta. As the proof-of-principle, we study cation order in the $Hf_6Nb_2O_{17}$ and determine the energetically most favorable structures. We also show that compositional sublattice modulation is correctly reproduced within this framework and establish a link between the oxygen sublattice modulation vector and cation composition.

2 | METHODS

Samples were fabricated using standard solid-state synthesis techniques like those described in ref.[12] Pure hafnia (3N5) and niobia (4N) powders were weighed into 13 separate batches with different compositions according to $Hf_nNb_2O_{2n+5}$ (n = 1–13). The powders were then milled in an ethanol for 9 h using a vibratory mill with toughened zirconia media. Powders were dried and pressed into pellets before calcining in a box furnace at 1050°C for 12 h. The pellets were then ground in a mortar and pestle

and subsequently milled again for 9 h. Pellets were then pressed at 5 000 lbs, embedded in a top and bottom layer of calcined powder and annealed at 1300°C for 12 h. After X-ray characterization of the ceramic pellets, the samples were reground and the described routine was repeated for annealing temperatures of 1375°C and 1450°C.

X-ray diffraction was carried out with a *Rigaku Ultima IV* X-ray powder diffractometer equipped with a Cu source. Phase compositions for these samples were determined through Pawley fitting[13] to the X-ray data using the software package GSAS II.[14] Time-of-flight (TOF) neutron diffraction data were recorded with the POWGEN diffractometer at beamline 11A SNS of Oak Ridge National Laboratory.

First-principles' DFT was performed using the Quantum ESPRESSO code. All calculations were done within the generalized gradient approximation with the Perdew–Burke–Ernzerhof (PBE) functional. Plane-wave energy cutoffs of 540 eV and a $4 \times 4 \times 2$ k-point were used. Structural optimization is carried out until all Cartesian forces on the ions are less than 4 meV/Å and the total energy difference between structural relaxation iterations is below 1 meV.

Interatomic potentials of classical Morse and Beest–Kramer–van Santen (M-BKS) character were chosen for our force-field model. Combining these potentials has been shown to provide good results in hafnia and tantalum pentoxide before and is thus expected to perform well here too.[15] The interatomic potentials have been optimized to our material system by taking the literature potential parameters as starting point and using the GULP software package[16] to fit the parameters to accurately predict the structure of $Hf_nNb_2O_{2n+5}$ (n = 1–7), as well as the bulk structures of Nb_2O_5 and HfO_2, as calculated by DFT.

3 | RESULTS

3.1 | Stability range of solid-state synthesized ceramics

Figure 1B shows exemplary X-ray scans of three different samples prepared at 1300°C: 71.4%, 85.7%, and 90.9% HfO_2. Note that all HfO_2 percentages are expressed in mole percent throughout this paper. In order to determine the actual phase compositions, three different phases are considered: the two parent compounds, monoclinic HfO_2 and h-Nb_2O_5, as well as $Hf_6Nb_2O_{17}$ (Figure 1A). The crystal structure of the latter was taken from the work of McCormack and Kriven.[17] We found that the XRD scan of the 85.7% sample could be fit solely with the $Hf_6Nb_2O_{17}$, that is, this sample is phase pure. However, the 71.4% and 90.9% samples were mixed phase. It should be stressed
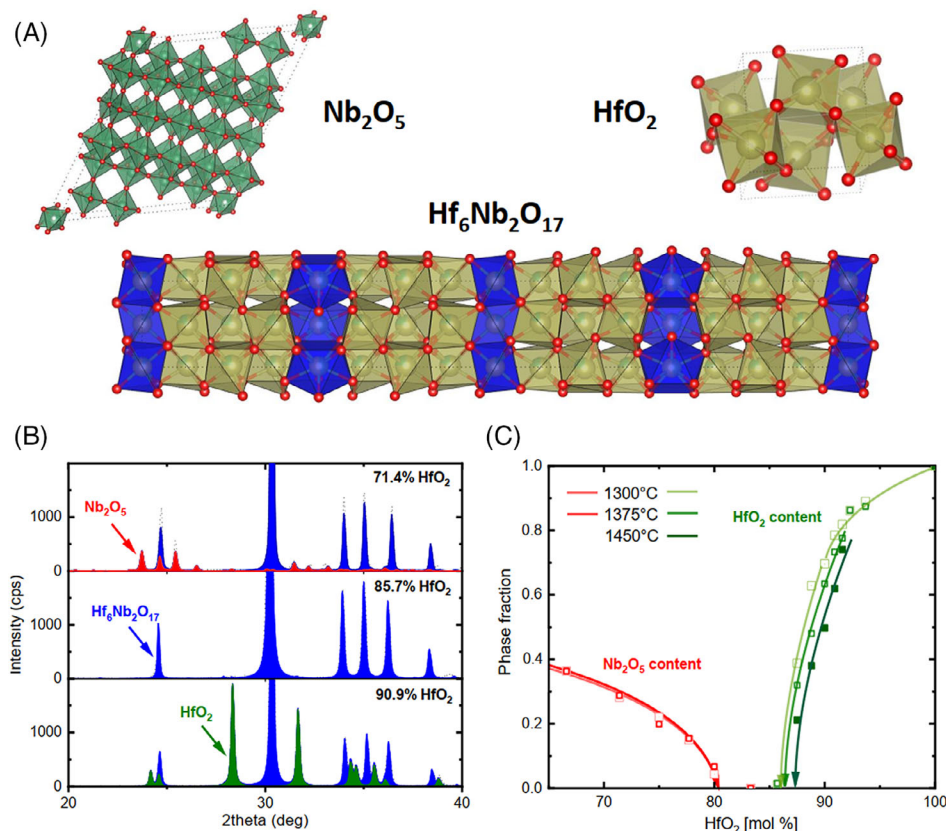
FIGURE 1 (A) Crystal structures of the three phases used to refine XRD data, that is, monoclinic h-Nb_2O_5, monoclinic HfO_2, and orthorhombic $Hf_6Nb_2O_{17}$. (B) Exemplary results of a XRD refinement for three different compositions sintered at 1 300°C with varying content of the three phases. Peaks stemming from different phases are shaded in different colors for clarity. (C) Determined phase fractions of h-Nb_2O_5 and HfO_2 as a function of the nominal HfO_2 content for various sintering temperatures. Solid lines are fits to the data.

that our XRD fitting approach does not allow to report phase contents with high confidence (< a couple per cent) and generally an internal standard, such as Si or corundum, would be needed. However, the $Hf_nNb_2O_{2n+5}$ phase stability range can be determined with good accuracy by extrapolating the contents of Nb_2O_5 and HfO_2 to zero, since this approach renders the need for a reference unnecessary. Figure 1C shows the determined parent compound phase contents as a function of the nominal HfO_2 content in the HfO_2–Nb_2O_5 system. It can be seen that the contents of the parent compounds generally decrease toward the stability region of the homologous series. The solid lines are fits to the experimental data where the phase content follows the theoretically expected fraction of Nb_2O_5 and HfO_2, that is, left after the complete reaction to the lower and higher $Hf_nNb_2O_{2n+5}$ bound phase, respectively. That means the stability limits are fitting parameters. For the 1300°C series, we find the $Hf_nNb_2O_{2n+5}$ phase to be stable between 80.5% and 86.0% HfO_2, that is, for n values between 4.1 and 6.2. With increasing temperature the upper limit of the stability region appears to slightly shift toward higher HfO_2 contents, while the lower limit remains unchanged. It should be noted that at 1450°C

unreacted Nb_2O_5 powder started to melt and thus, phase content data determined from XRD scans would be unreliable. We have therefore omitted these data from the graph. The upper phase stability limit for this temperature has shifted to 87.3%. Widening of the stability region is expected to be observed as increasing temperatures and additional milling steps increases the reaction of unreacted hafnia and niobia powder. The shift toward higher HfO_2 contents, however, indicates that at higher temperatures stoichiometric changes due to Nb-loss might be an issue. Similar observations have been reported before.[10] A consequence would be that practically $Hf_nNb_2O_{2n+5}$ compounds are better prepared via low-temperature routes that rely on shorter ion diffusion processes as opposed to high-temperature solid-state synthesis.

3.2 | Stability range from density-functional theory calculations

In order to corroborate the experimental results, DFT calculations have been performed. A good agreement between experimental and theoretical studies would imply
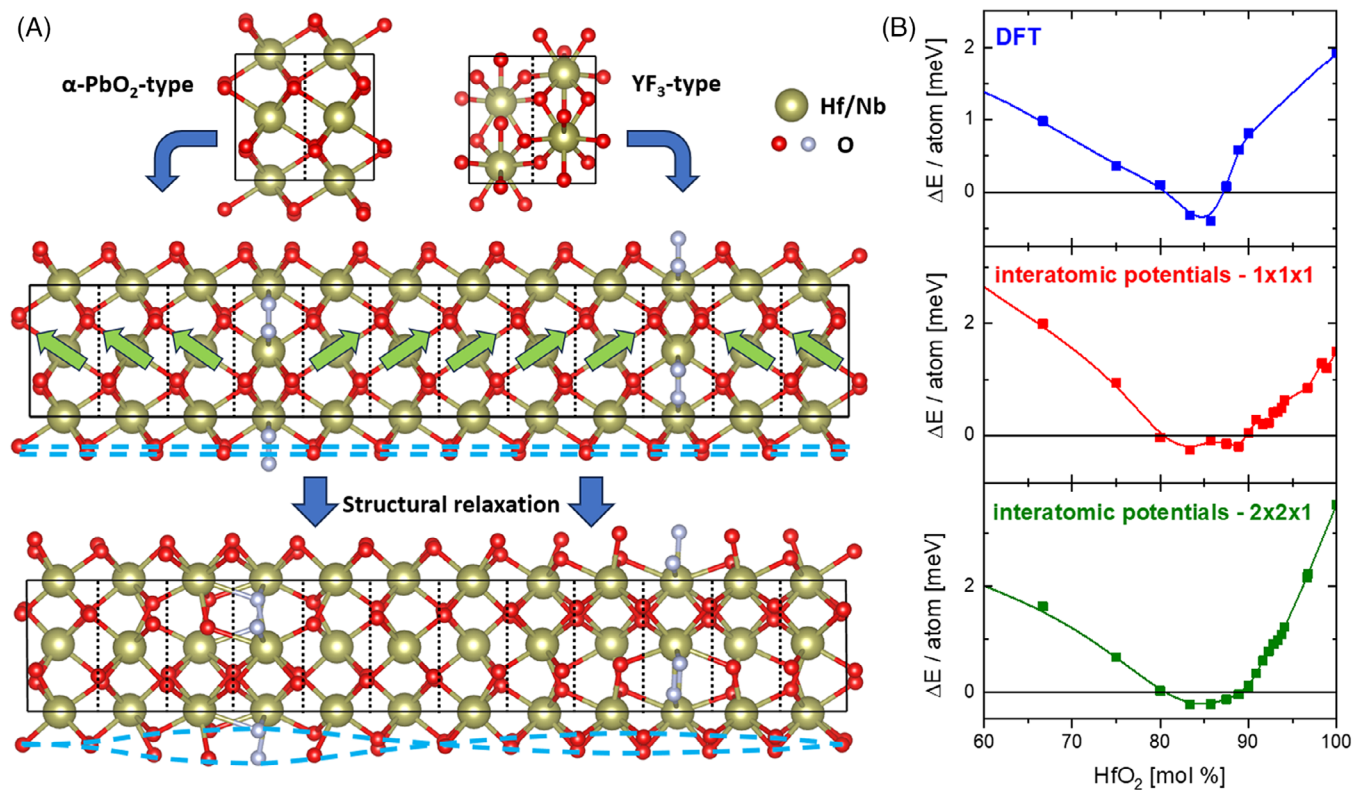
FIGURE 2 (A) Framework for structural relaxation of $A_nB_2O_{2n+5}$ phases within the DFT and interatomic potentials approach. The starting configuration is composed of $2(n+1)$ slabs with α-PbO_2-type structure and two slabs of the YF_3-type structure. As indicated by the green arrows, the orientation of the trigonal oxygen prisms flips at these intermittent slabs. After structural relaxation, the $A_nB_2O_{2n+5}$ phase is well reproduced. A periodic nearly sinusoidal displacement of the oxygen ions is observed (blue dashed line). (B) Formation energies compared to the two parent compounds as a function of the molar HfO_2 content for the DFT and the interatomic potentials based calculations with a $1 \times 1 \times 1$ and $2 \times 2 \times 1$ supercell, respectively. DFT, Density functional theory.

that the theory approach can be applied to not only this material systems but also other related material systems and can be used to predict material characteristics that are not easily accessible by experiment, which is of particular importance for high-temperature systems. The stability range of the homologous series is determined by structurally relaxing an "ideal" parent crystal structure to minimize its ground-state total energy. This total energy is then compared to the total energy of the according phase mixture of HfO_2 and Nb_2O_5. Figure 2A shows the starting crystal configuration of the "ideal" $Hf_nNb_2O_{2n+5}$ crystal structure. For example, the configuration for $n = 4$ is composed of a total of $2(n+2) = 12$ α-PbO_2-type unit cell blocks. The α-PbO_2-type structure is characterized by a highly distorted octahedral arrangement of oxygen anions with three inequivalent metal–oxygen bond distances.[18] For two of these blocks, two additional oxygen atoms are added. These additional atoms account for the additional oxygen, that is, brought into the system by Nb_2O_5, so that the overall charge state remains neutral. These blocks are equally spaced across the entire unit cell and resemble the YF_3-type structure which is characterized by a cation coor-

dination number of 9.[19] The capped trigonal oxygen prisms of the PbO_2 blocks change orientation at these oxygen-rich blocks and PbO_2-type blocks are simply added or deleted to create unit cells with higher or lower n, respectively. For a more detailed insight into the building principle of the homologous series, the reader is referenced to the original work of Galy et al.[9] or later descriptions by Wiedemann et al.[3] and McCormack and Kriven.[17] The Hf and Nb cations are randomly distributed over the metal ion sites according to their phase content. The bottom part of Figure 2A shows the crystal structure of the $n = 4$ configuration after structural relaxation. We find a very good agreement with the crystal structure reported by McCormack et al.,[17] with unit cell volume and average atomic positions differences of only 0.4% and 0.04 Å, respectively.

In Figure 2B, the formation energy per atom versus the hafnia and niobia parent compounds is plotted as a function of the nominal HfO_2 content for all studied members of the homologous series. For the calculations performed by DFT, the graph implies that the $n = 6$ member (85.7% HfO_2) is the most stable compound within the homologous series. This observation has been made also

experimentally for all $A_nB_2O_{2n+5}$. It can also be seen that between 80.5% and 87.5% the formation of the $Hf_nNb_2O_{2n+5}$ phase is energetically favored. This result agrees well with the experimentally measured stability limits.

3.3 | Stability range from force-field calculations

Since the DFT calculations assume that periodic boundary conditions and the unit cells used to calculate $Hf_nNb_2O_{2n+5}$ properties are only one α-PbO$_2$ block wide, the calculated structures are technically cation ordered along the a and b crystal axes. True disorder would require large supercells along all Cartesian axes which is too computationally expensive for DFT. For this reason, we have developed a force-field model based on classical interatomic potentials. In terms of accuracy, classical force fields typically perform quite well for predominantly ionic materials, while they are still computationally highly efficient. This fact allows one to move away from a single unit cell and conveniently study large supercells containing thousands of atoms. The middle panel of Figure 2B shows the result for the single unit cell using interatomic potentials. The stabilization of $Hf_nNb_2O_{2n+5}$ between roughly 80% and 89% is well reproduced, but the data are noisy. In a second step, we performed the same calculations for $2 \times 2 \times 1$ supercells (lower panel), meaning that the unit cells were doubled in size along the a and b crystal direction. This supercell provides configurations that are much closer to true random cation disorder, where effects of period boundary conditions are negligible. Consequently, the noise is reduced and a smooth curve with a stability region between 80.5%–89% is obtained. Overall, the DFT results are in good agreement with the force-field calculations. This fact indicates that our interatomic potentials can be used to study other characteristics of the $Hf_nNb_2O_{2n+5}$ system.

3.4 | Cation order

The question of cation order in $A_nB_2O_{2n+5}$ has been under debate for some time. The currently accepted position is that all four ternary variants show complete disorder on the metal ion site.[17] Our XRD data do not present additional reflections that would show up under any kind of cation order and therefore corroborates this finding. The computational demand of DFT is too great to study the large configurational space within the large unit cells of $A_nB_2O_{2n+5}$. However, our framework using interatomic potentials makes global optimization schemes which mini-
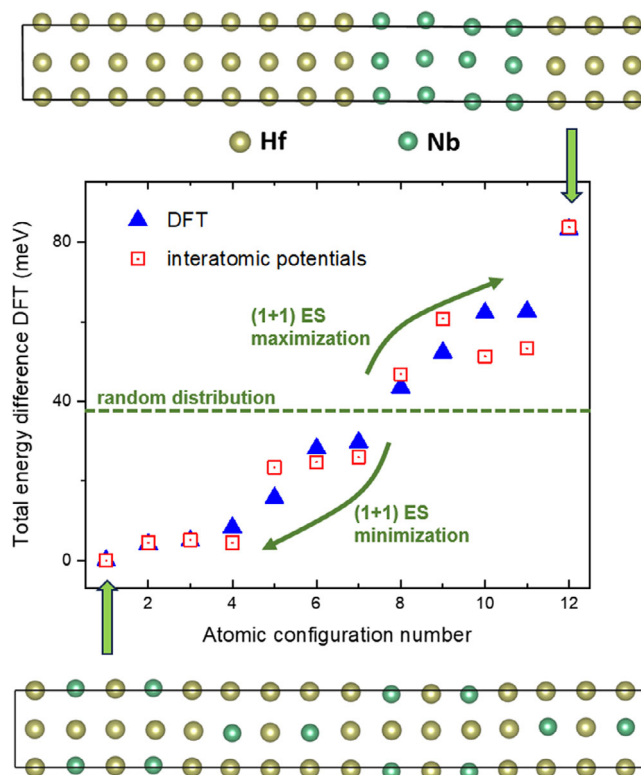
FIGURE 3 Global minimization and maximization of formation energy with respect to cation order using interatomic potential based calculations and a $1 \times 1 \times 1$ supercell. DFT calculations have been performed for the 12 exemplary configurations in order to showcase the good agreement between the two calculation types. DFT, Density functional theory.

mize the energy configuration computationally accessible. As proof-of-principle, we have applied a simple optimization algorithm, the (1+1) evolution strategy,[20] to $1 \times 1 \times 1$ and $2 \times 2 \times 1$ supercells of $Hf_6Nb_2O_{17}$ and determined the cation order configurations with the lowest and highest formation energies.

Within the evolutionary process of the $1 \times 1 \times 1$ supercell it took about 10 000 steps to reach the end points with maximal and minimal formation energies, starting from a random distribution. For 12 of these configurations within the optimization path, the formation energies were also calculated with DFT and the results are plotted in Figure 3. The very good agreement with the interatomic potential calculations demonstrates the reliability of this approach. The highest formation energy is obtained when Hf and Nb cations perfectly separate into slabs of HfO$_2$ and Nb$_2$O$_5$, as illustrated in the top part of Figure 3. This result validates that the interdiffusion of Hf and Nb ions into their parent counterparts is thermodynamically favored. In the energetically lowest cation arrangement, every second plane of cations is comprised of only Hf ions, while for the remaining planes the Hf and Nb ions are distributed in a regular checkerboard type pattern (bottom part of

Figure 3). It is noteworthy that the evolutionary energy minimization of the $2 \times 2 \times 1$ supercells leads to the same cation arrangements.

We emphasize again that the lack of XRD superlattice peaks highlights the absence of cation order in our sintered samples, which is a result of the high entropy of the system. This observation may be reflected in the progression of cation ordering states during solid-state synthesis methods. In the early stages of phase stabilization, the cation configuration would be similar to the described structure shown for configuration number of 12, which is characterized by separate slabs of Hf and Nb ions. During annealing, as a function of time and temperature the driving force for free enthalpy minimization would result in the intermixing of Hf and Nb ions. While the energetically most favorable state is cation ordered, the relative energy differences between different cation configurations are small and are overcome by the entropy component to the free enthalpy at high sintering temperatures. In consequence, the structure approaches a randomly mixed configuration. Our calculations are supporting this scenario.

3.5 | Periodically modulated structure

In the first structural description by Galy and Roth,[9] the $A_nB_2O_{2n+5}$ phases were described within the context of a discrete homologous series. It was later realized that a compositionally modulated superstructure consisting of two independent sublattices, that is, the cation lattice and the oxygen lattice, would better explain XRD and neutron diffraction data. In this scenario, the ions are systematically misplaced from their average position whereby this misplacement can be described as a periodic modulation. The wavelength λ of this periodic modulation is composition dependent and allows for the continuous variation in phase space, as opposed to the homologous series formalism. As example, the periodic modulation of the oxygen sublattice is highlighted for $Hf_4Nb_2O_{13}$ in Figure 2A as dashed blue line. In this specific case, the periodicity λ of the periodic modulation is 12 α-PbO$_2$-type blocks.

As a way to highlight the features of this compositionally modulated structure in Figure 4, we have analyzed neutron data of an 85% HfO_2–15% Nb_2O_5 sample sintered at 1 500°C. In order to achieve the right stoichiometry, an 85% sample can be thought of as consisting of members of the homologous series with two unit cells of $Hf_6Nb_2O_{17}$ and one unit cell of $Hf_5Nb_2O_{15}$, that is, leading to a structure with 46 α-PbO$_2$ type blocks and an $Hf_{17}Nb_6O_{49}$ formula unit. Consequently, the expected modulation periodicity is $46/3 = 15.3$ α-PbO$_2$ type blocks. To fit the neutron diffraction data, we have therefore refined an $Hf_nNb_2O_{2n+5}$ superstructure with a constant
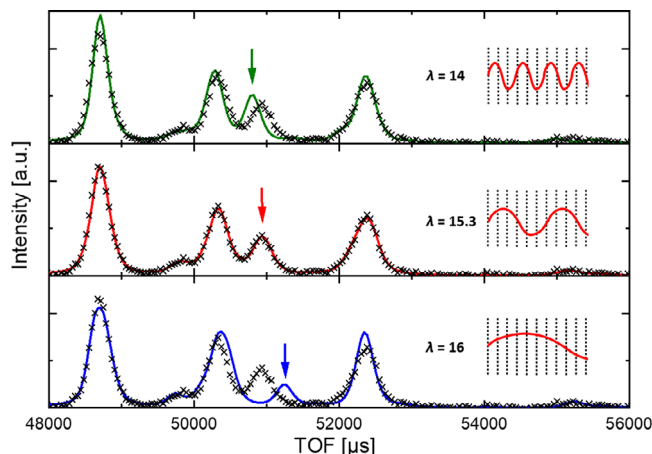
FIGURE 4 Refinement of three different crystal superstructures to neutron diffraction data of an 85% HfO_2–15% Nb_2O_5 sample sintered at 1500°C. Black points represent measured data, while colored solid lines are simulated scans based on the refined crystal structures. The three crystal structures used as a starting point to the refinement are based on $Hf_nNb_2O_{2n+5}$ with a fixed oxygen sublattice modulation periodicity of $\lambda = 14$ (top), 15.3 (middle), and 16 (bottom). The insets schematically illustrate the modulation of the oxygen ion positions (not to scale).

sublattice periodicity of $\lambda = 15.3$ (Figure 4, middle). An almost perfect fit was achieved. When a different λ of 14 (top) and 16 (bottom) is assumed, the fits are less satisfactory. In particular, the peak at around 51 000 μs is attributed to the modulated oxygen sublattice and is only captured well when the periodicity of the modulation is correct. For larger and smaller λ values, the peak is shifted to higher and lower TOF, respectively. It should be noted too that the presence of only one single peak at 51000 μs directly corroborates the existence of a compositionally homogenous single-phase state. If the 85% sample would be made up of a compositionally adjusted ratio of the $Hf_5Nb_2O_{15}$ and $Hf_6Nb_2O_{17}$ members of the homologous series, separation into two distinguished peaks would be expected.

Our framework using interatomic potential successfully reproduces the characteristics of a periodically modulated phase. In order to showcase this fact, we have calculated the energies of $1 \times 1 \times 15$ supercells for various compositions as a function of their oxygen sublattice modulation wavelength. As can be seen in Figure 5, for all integer $Hf_nNb_2O_{2n+5}$ compositions pronounced energy minima are formed when λ is congruent with $2(n+2)$ building blocks. This fact basically means that for these compositions all structures relax from there uniform starting point towards commensurate end points as described by the homologous series. This is noteworthy since due to the supercell approach and the continuous variation of λ no implicit symmetry was enforced.
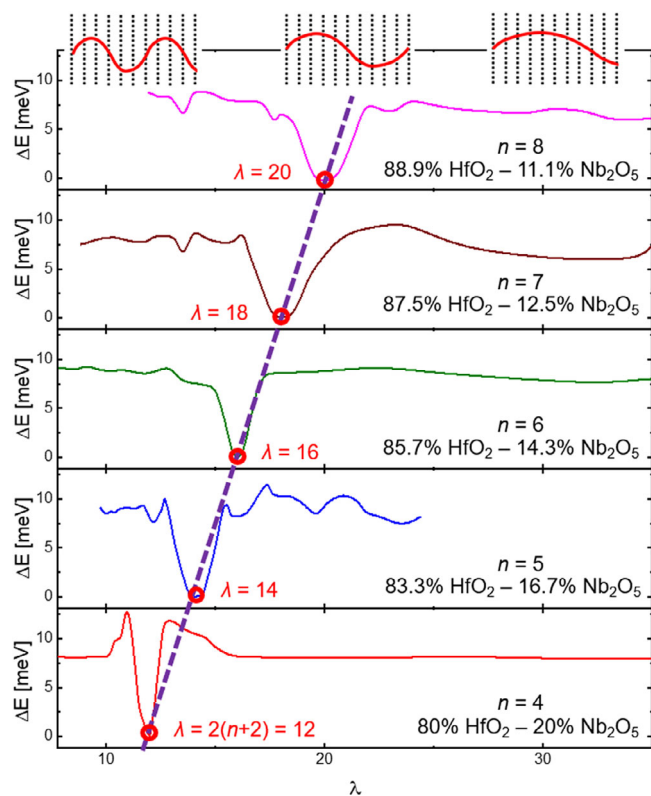
FIGURE 5 Formation energy as a function of λ in units of α-PbO$_2$-type unit blocks assuming a sinusoidal wave (schematically shown at the top). The energies are plotted with respect to their energetically most stable configurations (red circles) that are found to coincide with the discrete members of the $A_nB_2O_{2n+5}$ homologous series. Large $1 \times 1 \times 15$ supercells were used to allow for a smooth variation of the modulation vector.

4 | CONCLUSIONS

Research on high-temperature ceramic materials is of considerable interest for emerging technologies in energy and aerospace systems. This work explores the $A_nB_2O_{2n+5}$ phase within the AO_2–B_2O_5 system which has great potential due to high melting temperatures and robust chemical stability. Here, we have developed an experimental and theoretical framework to study important characteristics of the $Hf_nNb_2O_{2n+5}$ phase. In particular, it was confirmed that the $Hf_nNb_2O_{2n+5}$ phase is thermodynamically stable over a range of roughly 80.5–87.5 mol % HfO_2. A force-field model based on classical interatomic potentials was developed and shown to reach accuracies comparable to DFT approaches. This framework was then applied to study the effects of cation order and compositional periodic modulation. In the future, our model could be used in molecular dynamics calculations to explore other characteristics, such as thermodynamic expansion or melting temperatures. An extension to include other dopants should be feasible without a large computational effort.

ORCID

Andreas Herklotz https://orcid.org/0000-0002-1545-131X

Kyle Martin Grove https://orcid.org/0000-0002-9518-1232

Michael S. Bowen https://orcid.org/0000-0001-7801-9420

REFERENCES

1. Rana HM. A review paper on thermal barrier coatings (TBC) to improve the efficiency of gas turbine. Int J Sci Res Dev. 2016;4:1161–65.
2. Zhang MH, Rhee SJ, Kang CY, Choi CH, Akbar MS, Krishnan SA, et al. Improved electrical and material characteristics of HfTaO gate dielectrics with high crystallization temperature. Appl Phys Lett. 2005;87(23):232901.
3. Wiedemann D, Lüdtke T, Palatinus L, Willinger E, Willinger MG, Mühlbauer MJ, et al. At the gates: the tantalum-rich phase Hf$_3$Ta$_2$O$_{11}$ and its commensurately modulated structure. Inorg Chem. 201857(22):14435–42.
4. Schroeder U, Park MH, Mikolajick T, Hwang CS. The fundamentals and applications of ferroelectric HfO$_2$. Nat Rev Mater. 2022;7(8):653–69.
5. Aamlid SS, Oudah M, Rottler J, Hallas AM. Understanding the role of entropy in high entropy oxides. J Am Chem Soc. 2023;145(11):5991–6006.
6. Voskanyan AA, Lilova K, McCormack SJ, Kriven WM, Navrotsky A. A new class of entropy stabilized oxides: commensurately modulated A$_6$B$_2$O$_{17}$ (A = Zr, Hf; B = Nb, Ta) structures. Scr Mater. 2021204:114139.
7. McCormack SJ, Tseng KP, Weber RJK, Kapush D, Ushakov SV, Navrotsky A, et al. In-situ determination of the HfO$_2$–Ta$_2$O$_5$-temperature phase diagram up to 3000°C. J Am Ceram Soc. 2019102(8):4848–61.
8. Roth RS, Waring JL, Brower WS, Parker HS. Superstructure of the orthorhombic Nb$_2$O$_5$·6ZrO$_2$ type phase(s) in the Nb$_2$O$_5$–ZrO$_2$ and Ta$_2$O$_5$–ZrO$_2$ system. Natl Bur Stand. 1972;(364):183–95.
9. Galy J, Roth RS. The crystal structure of Nb$_2$Zr$_6$O$_{17}$. J Solid State Chem. 1973;7(3):277–85.
10. Thompson JG, Withers RL, Sellar J, Barlow PJ, Hyde BG. Incommensurate composite modulated Nb$_2$Zr$_x$−2O$_{2x+1}$: x = 7.1–10.3. J Solid State Chem. 1990;88(2):465–75.
11. Futterer K, Schmid S, Thompson JG, Withers RL, Ishizawa N, Kishimoto S. The structure refinement of compositely modulated Nb$_2$Zr$_{x2}$O$_{2x+1}$ (x = 12). Acta Crystallogr B. 1995;51:688–97.
12. Bowen MS, Johnson M, McQuade R, Wright B, Kwong KS, Hsieh PY, et al. Electrical properties of gadolinia-doped ceria for electrodes for magnetohydrodynamic energy systems. SN Appl Sci. 2020;2(9):1529.

13. Pawley G. Unit-cell refinement from powder diffraction scans. J Appl Crystallogr. 1981;14(6):357–61.

14. Toby BH, Von Dreele RB. GSAS-II: the genesis of a modern open-source all-purpose crystallography software package. J Appl Crystallogr. 2013;46:544–49.

15. Trinastic JP, Hamdan R, Wu Y, Zhang L, Cheng HP. Unified interatomic potential and energy barrier distributions for amorphous oxides. J Chem Phys. 2013;139(15):154506.

16. Gale JD, Rohl AL. The general utility lattice program (GULP). Mol Simul. 2003;29(5):291–341.

17. McCormack SJ, Kriven WM. Crystal structure solution for the $A_6B_2O_{17}$ (A = Zr, Hf; B = Nb, Ta) superstructure. Acta Crystallogr B. 2019;75:227–34.

18. Aamlid SS, Johnstone GHJ, Mugiraneza S, Oudah M, Rottler J, Hallas AM. Phase stability of entropy stabilized oxides with the α-PbO$_2$ structure. Commun Mater. 2023;4(1):45.

19. Micale C, Almeida RM. Structure and properties of Er and Er/Yb-doped YF$_3$ up-conversion phosphors compared with oxide hosts through an internal standard. Mater Today Commun. 2022;31:103239.

20. Droste S, Jansen T, Wegener I. On the analysis of the (1+1) evolutionary algorithm. Theor Comput Sci. 2002;276(1):51–81.